Free Vibration Analysis of Laminated CNTRC Plates using the pb2-Ritz Method

Dang Xuan Hung, Tran Minh Tu, Tran Dai Hao*
National University of Civil Engineering, 55 Giai Phong Road, Hanoi, VN
**tutm@nuce.edu.vn*

ABSTRACT

This paper presents the free vibration analysis of laminated functionally graded carbon nanotube reinforced composite (FG-CNTRC) plates. The CNTRC layer consists of single-walled carbon nanotubes (SWCNTs) as reinforcement and polymer as a matrix. The material properties are determined according to the extended rule of mixture. Four different patterns of SWCNTs distribution across the thickness of individual layers are considered. Based on the first-order shear deformation theory (FSDT), the equations of motion are derived and then solved by employing the pb2-Ritz method. The accuracy of the present approach is verified by comparing the obtained results with those available in the literature and commercial ANSYS software. The significant influences of CNT volume fractions, CNT distribution patterns, plate aspect ratio, plate width-to-thickness ratio, and boundary conditions on the non-dimensional fundamental frequency of symmetric and anti-symmetric laminated FG-CNTR plates has been proven through the numerical examples. Furthermore, the influence of lamination schemes, CNT fiber orientation and the number of layers is also investigated.

Keywords: *Laminated carbon nanotube-reinforced composite; Free vibration analysis; First-order shear deformation theory; pb2-Ritz method.*

Introduction

Since they were invented in 1991 by Iijima [1], carbon nanotubes (CNTs) have been increasingly used in many modern industries due to their exceptional mechanical, thermal and electrical properties. Therefore, the CNTs are used as a new type of reinforcement of polymer composite that has the potential to replace traditional reinforcement materials for structural components. With the

ISSN 1823-5514, eISSN 2550-164X
Received for review: 2020-08-24
Accepted for publication: 2021-01-06
Published: 2021-01-15

idea of functionally graded (FG) materials, CNTs have been distributed continuously through the matrix along the certain direction of composite structures. Functionally graded carbon nanotube-reinforced composites (FG-CNTRCs) can be applied as structural members such as beam, plate or shell in many engineering branches such as mechanical, aeronautical, civil, and marine industries. In order to optimize the design of CNTRC's structures, a thorough understanding of their mechanical behavior is required. Thus, the study on vibrational characteristics of these structures always attracts the attention of design engineers.

The mechanical behavior of single-layer FG and FG-CNTRC structures has been studied by many researchers. Based on first-order shear deformation theory (FSDT), Bidgoli et al. presented a three-dimensional thermo-elastic analysis [2], two-dimensional stress and strain behavior [3] of a rotating FG cylindrical shell subjected to inner and outer pressures; Zhu et al. [4] investigated the static and free vibration characteristics of FG-CNTRC plates by the FEM. Using Ritz method, Shahrbabaki and Alibeigloo [5] analyzed the free vibration of FG-CNTRC plates with various boundary conditions. Nami and Janghorban [6] studied the free vibration of FG-CNTRC plates using the differential quadrature method (DQM) and the theory of elasticity. Adopting the generalized DQM and Galerkin's technique, the forced vibration of FG-CNTRC plates based on the FSDT was analyzed by Ansari et al. [7]. Selim et al. [8] adopted the element-free kp-Ritz method to study the free vibration behavior of FG-CNTRC plates including thermal effect based on Reddy's higher-order shear theory (HSDT). Zhang [9] employed the element-free IMLS-Ritz method and FSDT to analyze the vibrational characteristics of FG-CNTRC triangular plates. Using the same method, Zhang et al. [10-12] presented the vibration analysis of FG-CNTRC thick and moderately thick plates using the FSDT and HSDT. Using DQM, the free vibration and static behavior of FG-CNTRC plate was studied by Alibeigloo and Emtehani [13]. Using HSDT and the state-space Levy solution, Zhang et al. [14] investigated the vibration response of FG-CNTRC plates subjected to in-plane loads. Using a variational differential quadrature approach, Ansari et al. [15] analyzed the free vibration of arbitrary shaped thick FG-CNTRC plates based on the HSDT.

The Ritz method, an effective tool to solve a system of differential equations, was applied by Kiani [16] to study the free vibration of FG-CNTRC skew plates plates. Wang et al. [17] presented Kantorovich-Galerkin method for free vibration and buckling analysis of FG-CNTRC thin plates with the Kirchhoff plate theory. Duc et al. [18] discussed the bending and free vibration of FG-CNTRC rectangular plates resting on Winkler-Pasternak elastic foundations using the FSDT. The cell-based smoothed discrete shear gap method (CS-DSG3) for the bending and free vibration analyses of FG-CNTRC rectangular plates is proposed by Tam et al.[19]. Using the element-

free kp-Ritz method, the free vibration analysis of laminated FG-CNTRC plates were studied by Lei et al. [20] based on the FSDT.

As is well-known, multi-layer composite structures are more commonly used than single-layer composite structures. The advantage of these structures is the motivation for scientists to understand thoroughly the mechanical behavior of laminated FG-CNTRC beams, plates and shells, whose bearing capacity depends on many parameters such as CNT configurations, CNT orientations, and number of layers. However, so far there have not been many studies on this topic; only a few studies have been introduced. Malekzadeh and Zarei [21] predicted natural frequencies of quadrilateral multi-layered FG-CNTRC plates using the DQM and the FSDT. Free vibrational behaviors of FG-CNTRC and laminated FG-CNTRC plates under different boundary conditions based on Reissner's mixed variational theorem using finite prism methods was analyzed by Wu and Li [22]. Malekzadeh and Heydarpour [23] employed the layerwise-DQM to study static and free vibration analysis of laminated FG-CNTRC plates. Based on a simple four-variable FSDT, Huang et al. [24] used the Navier solution to solve bending and free vibration problems of anti-symmetrically laminated FG-CNTRC plates. Lei et al. [25] investigated static behaviors of laminated FG-CNTR plates by the element-free kp-Ritz method.

An above-mentioned review shows that there are very few researches on the vibrational characteristics of CNTRC multi-layered composite plates using a Rayleigh-Ritz procedure that does not require topological discretization. For the Rayleigh-Ritz method, there is difficulty in choosing a suitable Ritz displacement function for plates with arbitrary supporting edges such that it can be easily automated. The pb2-Ritz function consists of the products of the two-dimensional polynomial functions and the basic boundary functions. As a result, this method can be easily automated and requires less computer memory space due to the reduction of unknowns.

In this paper, the pb-2 Rayleigh-Ritz method is applied to find a solution for the free vibration problem of laminated FG-CNTRC plates under various boundary conditions for the first time. The convergence test is conducted to illustrate the accuracy of the present approach. In addition, the effects of volume fraction of CNTs, different CNT distributions, lamination schemes, geometric parameters of the plate, and boundary conditions on the natural frequency parameters are investigated.

Laminated FG-CNTRC plates

In this article, a multi-layered rectangular plate of length *a*, width *b* and total thickness *h* is considered. The plate composed of the FG-CNTRCs layers, which are perfectly bonded (Figure 1). It is assumed that the individual layers are made of a mixture of SWCNTs (single-walled CNTs) and an isotropic matrix. The Cartesian coordinate system, four patterns of CNT distribution

along the thickness of the layer are also illustrated in Figure 1. The conventional single-walled CNT (SWCNT) distributions are assumed to be graded along the thickness direction and represented by four types of distribution: the uniform distribution (UD), and other three functionally graded distributions are denoted as FG-V, FG-X and FG-O respectively.

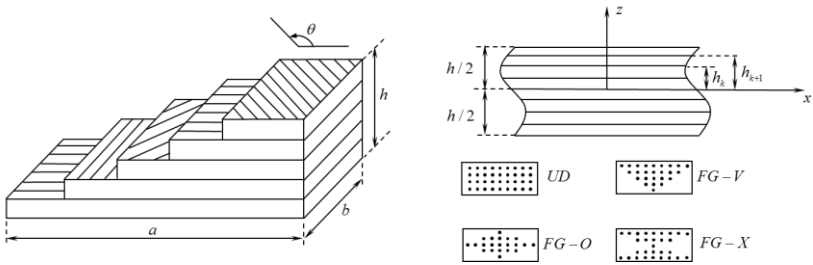

Figure 1: Geometry and configuration of laminated FG-CNTRC plate with different types of CNT distributions through layer's thickness.

The CNT volume fractions for each FG-CNTRC layer can be determined according to the types of CNT's distributions as [26]:

$$V_{CNT} = V_{CNT}^{*} \quad (\text{UD}); \; V_{CNT}(z) = \left(1 - \frac{2|z|}{h}\right) V_{CNT}^{*} \quad (\text{FG-O})$$

$$V_{CNT}(z) = \left(1 + \frac{2z}{h}\right) V_{CNT}^{*} \; (\text{FG-V}); \; V_{CNT}(z) = \frac{4|z|}{h} V_{CNT}^{*} \quad (\text{FG-X}) \tag{1}$$

with,

$$V_{CNT}^{*} = \frac{w_{CNT}}{w_{CNT} + \left(\rho^{CNT} / \rho^{m}\right) - \left(\rho^{CNT} / \rho^{m}\right) w_{CNT}} \tag{2}$$

in which ρ^{CNT} and ρ^{m} are the densities of the CNTs and the matrix respectively; w_{CNT} is the mass fraction of the CNT.

The effective CNTs properties can be approximated using the Eshelby–Mori–Tanaka scheme [27] or the extended rule of mixture [28]. In the present research, the extended rule of mixtures is chosen for simplicity, and effective Young's modulus, shear modulus, Poisson's ratio and density of CNTRC layers can be expressed as:

$$E_{11} = \eta_1 V_{CNT} E_{11}^{CNT} + V_m E^m;\ \frac{\eta_2}{E_{22}} = \frac{V_{CNT}}{E_{22}^{CNT}} + \frac{V_m}{E^m};\ \frac{\eta_3}{G_{12}} = \frac{V_{CNT}}{G_{12}^{CNT}} + \frac{V_m}{G^m}; \quad (3)$$
$$\nu_{12} = V_{CNT}^{*} \nu_{12}^{CNT} + V_m \nu^m;\quad \rho = V_{CNT}\rho^{CNT} + V_m \rho^m$$

where $E_{11}^{CNT}, E_{22}^{CNT}$ and G_{12}^{CNT} are the Young's and shear moduli of single-walled carbon nanotubes (SWCNTs) in the principal material coordinate, respectively; E^m and G^m are the corresponding properties of the isotropic matrix; η_1, η_2, and η_3 are the CNT efficiency parameters; V_{CNT} and V_m are the volume fractions of the CNTs and polymer matrix, respectively. ν^m, ρ^m are the Poisson's ratio, the density of the CNT and the polymer matrix, respectively.

Theoretical formulation

First-order shear deformation theory (FSDT)

The in-plane displacement components and the transverse displacement component according to the FSDT can be assumed as [29]:

$$\begin{aligned} \bar{u} &= u(x,y) + z\theta_x(x,y) \\ \bar{v} &= v(x,y) + z\theta_y(x,y) \\ \bar{w} &= w(x,y) \end{aligned} \quad (4)$$

in which u, v, w are in-plane and the transverse displacements of a point on the mid-plane following the (x, y, z) directions, respectively; θ_x, θ_y are the rotations of the transverse normal about the y- and x-axes, respectively.

The nonzero strains associated with the displacement field (5) are given as:

$$\bar{\boldsymbol{\varepsilon}} = \begin{Bmatrix} \bar{\varepsilon}_{xx} \\ \bar{\varepsilon}_{yy} \\ \bar{\gamma}_{xy} \end{Bmatrix} = \boldsymbol{\varepsilon} + z\boldsymbol{\kappa};\ \begin{Bmatrix} \gamma_{yz} \\ \gamma_{xz} \end{Bmatrix} = \boldsymbol{\gamma} \quad (5)$$

where,

$$\boldsymbol{\varepsilon} = \begin{Bmatrix} \partial u/\partial x \\ \partial v/\partial y \\ \partial u/\partial y + \partial v/\partial x \end{Bmatrix}; \boldsymbol{\kappa} = \begin{Bmatrix} \partial \theta_x/\partial x \\ \partial \theta_y/\partial y \\ \partial \theta_x/\partial y + \partial \theta_y/\partial x \end{Bmatrix}; \boldsymbol{\gamma} = \begin{Bmatrix} \dfrac{\partial w}{\partial y} + \theta_y \\ \dfrac{\partial w}{\partial x} + \theta_x \end{Bmatrix} \quad (6)$$

The stress-strain relations of the k^{th} - CNTRC layer are given as:

$$\begin{Bmatrix} \sigma_{xx} \\ \sigma_{yy} \\ \sigma_{xy} \\ \sigma_{yz} \\ \sigma_{xz} \end{Bmatrix}^{(k)} = \begin{bmatrix} \tilde{Q}_{11} & \tilde{Q}_{12} & \tilde{Q}_{16} & 0 & 0 \\ \tilde{Q}_{12} & \tilde{Q}_{22} & \tilde{Q}_{26} & 0 & 0 \\ \tilde{Q}_{16} & \tilde{Q}_{26} & \tilde{Q}_{66} & 0 & 0 \\ 0 & 0 & 0 & \tilde{Q}_{44} & \tilde{Q}_{45} \\ 0 & 0 & 0 & \tilde{Q}_{45} & \tilde{Q}_{55} \end{bmatrix}^{(k)} \begin{Bmatrix} \overline{\varepsilon}_{xx} \\ \overline{\varepsilon}_{yy} \\ \overline{\gamma}_{xy} \\ \gamma_{yz} \\ \gamma_{xz} \end{Bmatrix}^{(k)} \tag{7}$$

with $\tilde{Q}_{ij}$ are engineering constants of the transformed stiffness matrix for the k^{th} layer, and are defined by:

$$\left[\tilde{Q}\right]_k = \left[T\right]^{-1}\left[Q\right]_k\left[T\right]^{-T} \tag{8}$$

in which θ is the CNT angle of lamination, and the transformation matrix [T] related to the principal materials coordinates and the structural coordinates are defined in [29].

The engineering constants Q_{ij} of the stiffness matrix $\left[Q\right]_k$ for the k^{th} layer are given as follow:

$$\begin{aligned} &Q_{11} = \frac{E_{11}}{1-\nu_{12}\nu_{21}};\ \ Q_{12} = \frac{\nu_{12}E_{22}}{1-\nu_{12}\nu_{21}};\ \ Q_{22} = \frac{E_{22}}{1-\nu_{12}\nu_{21}}; \\ &Q_{44} = G_{23};\ \ Q_{55} = G_{13};\ \ Q_{66} = G_{12}; \end{aligned} \tag{9}$$

in which the effective Young's moduli, shear moduli in the principal material coordinate and Poisson's ratios of the CNTRC materials, respectively are determined from Eqs. (2), (3).

The strain energy of laminated FG-CNTRC plates is given as:

$$U = \frac{1}{2}\int_A \tilde{\boldsymbol{\varepsilon}}^T \boldsymbol{S}\tilde{\boldsymbol{\varepsilon}}dA; \tag{10}$$

in which:

$$\tilde{\boldsymbol{\varepsilon}} = \begin{Bmatrix} \boldsymbol{\varepsilon} \\ \boldsymbol{\kappa} \\ \boldsymbol{\gamma} \end{Bmatrix}; \boldsymbol{S} = \begin{bmatrix} A & B & 0 \\ B & D & 0 \\ 0 & 0 & \overline{A} \end{bmatrix} \tag{11}$$

The stiffness coefficients of laminated FG-CNTRC are defined as:

$$\begin{aligned}(A_{ij}, B_{ij}, D_{ij}) &= \sum_{k=1}^{N} \int_{h_k}^{h_{k+1}} \overline{Q}_{ij}^{k}(1, z, z^2)dz \qquad (i, j = 1,2,6)\\ \overline{A}_{ij} &= f\sum_{k=1}^{N} \int_{h_k}^{h_{k+1}} \overline{Q}_{ij}^{k}dz \qquad (i, j = 4,5)\end{aligned} \tag{12}$$

where f is the transverse shear correction factor; h_k, h_{k+1} are the coordinates from the mid-plane of the plate to the top and bottom surface of the k^{th} layer; N is the total number of layers.

The kinetic energy of laminated FG-CNTRC plates is given as:

$$K = \frac{1}{2}\int_{A}\int_{-h/2}^{h/2} \rho(z)(\dot{\bar{u}}^2 + \dot{\bar{v}}^2 + \dot{\bar{w}}^2)dzdA \tag{13}$$

where $\rho(z)$ is the mass density and $(\dot{\bar{u}},\ \dot{\bar{v}},\ \dot{\bar{w}})$ are the velocity components along with the (x, y, z) directions, respectively. The total energy function of laminated FG-CNTRC plates for free vibration analysis is expressed as:

$$\Pi = U - K \tag{14}$$

Pb2- Ritz method based on the FSDT plate theory

Adopting the FSDT in conjunction with geometric boundary conditions of Mindlin plate, the displacement components are represented as follow:

$$\begin{aligned}u(x,y) &= \sum_{i=1}^{m}\sum_{j=1}^{n} U_{ij}^{mn} f_{ij}(x,y)\psi^{u}(x,y)e^{i\omega t}\\ v(x,y) &= \sum_{i=1}^{m}\sum_{j=1}^{n} V_{ij}^{mn} f_{ij}(x,y)\psi^{v}(x,y)e^{i\omega t}\\ w(x,y) &= \sum_{i=1}^{m}\sum_{j=1}^{n} W_{ij}^{mn} f_{ij}(x,y)\psi^{w}(x,y)e^{i\omega t}\\ \theta_x(x,y) &= \sum_{i=1}^{m}\sum_{j=1}^{n} \theta_{ij}^{xmn} f_{ij}(x,y)\psi^{\theta_x}(x,y)e^{i\omega t}\\ \theta_y(x,y) &= \sum_{i=1}^{m}\sum_{j=1}^{n} \theta_{ij}^{ymn} f_{ij}(x,y)\psi^{\theta_y}(x,y)e^{i\omega wt}\end{aligned} \tag{15}$$

where $i=\sqrt{-1}$ and ω is the natural frequency; m and n are degrees of the mathematically complete two-dimensional polynomial space; $U_{ij}^{mn}, V_{ij}^{mn}, W_{ij}^{mn}, \theta_{ij}^{xmn}, \theta_{ij}^{ymn}$ are the unknown coefficients to be determined; the complete set of two-dimensional polynomials $f_{ij}(x,y)$ can be expressed as: $X^{i-1}Y^{j-1}$ $(i=1,2,3,...m;\ j=1,2,3,...n)$; $\psi^{\alpha}(x,y)$, $\left(\alpha=u,v,w,\theta_x,\theta_y\right)$ are the functions that satisfy the geometric boundary conditions (BCs) and are expressed as:

$$\psi^{\alpha}(x,y)=\prod_{k=1}^{n_e}\left[\Gamma_k(x,y)\right]^{\Omega_k} \tag{16}$$

with n_e is the number of supporting edges; Γ_k is the equation of the k^{th} supporting edge (Figure 2); Ω_k are the representative parameters of the BCs and are given in Table 1. In this study, four types of BCs are considered: clamped edge (C), simply supported edge (S) and free edge (F).

Table 1: Representative parameters of various boundary conditions

	Ω_k		
α	F	S	C
u, v, w	0	1	1
θ_x, θ_y	0	0	1

Through substituting Equation (15) into Equation (14) and applying the Ritz procedure to the total energy functional, the eigenvalue problem is obtained as:

$$\left(\tilde{\boldsymbol{K}}-\omega^2\tilde{\boldsymbol{M}}\right)\{\boldsymbol{X}\}=0 \tag{17}$$

where $\tilde{\boldsymbol{K}}$ is the stiffness matrix and $\tilde{\boldsymbol{M}}$ is the mass matrix. $\boldsymbol{X}$ is the unknown displacement coefficients $\left(U_{ij}^{mn}, V_{ij}^{mn}, W_{ij}^{mn}, \theta_{ij}^{xmn}, \theta_{ij}^{ymn}\right)$. The eigenvalue problem (17) is solved by using the standard eigenvalue algorithm provided in a Matlab's code.

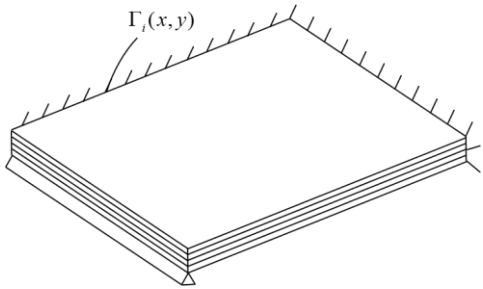

Figure 2: A rectangular laminated FG-CNTRC plate

Numerical Results and Discussions

In this section, after conducting convergence and accuracy of the solutions of the proposed method, the parametric studies will be performed to explore the effects of CNT volume fractions, length-to-width ratio, width-to-thickness ratio, CNT distribution pattern, fiber orientation, number of layers and boundary conditions on the natural frequencies of multi-layered FG-CNTRC plates.

Laminated FG-CNTR plates, whose each layer is made of poly{(m-phenylenevinylene)-co-[(2,5-dioctoxy-p-phenylene) vinylene] (PmPV) as matrix, with CNTs as fibers are considered. PmPV is an isotropic material with $\nu_m = 0.34$; $\alpha^m = 45\times10^{-6}K$; $E^m = 2.1$ GPa; $\rho^m = 1.15$ g/cm^3. The (10,10) single-walled carbon nanotubes (SWCNTs) are chosen as reinforcements, whose material properties are: $E_{11}^{CNT} = 5.6466$ TPa; $E_{22}^{CNT} = 7.0800$ TPa; $G_{12}^{CNT} = 1.9455$ TPa; $\rho^{CNT} = 1.4$ g/cm^3 [30]. The CNT efficiency parameters $\eta_j\,(j = 1,2,3)$, which are taken from Shen [30], are given in Table 2. In addition, the shear moduli are assumed as: $G_{13} = G_{12} = G_{23}$. These material properties will be used to perform the bellow numerical results.

Table 2: CNT efficiency parameters for three different value of volume fractions

V_{CNT}^*	η_1	η_2	η_3
0.11	0.149	0.934	0.934
0.14	0.150	0.941	0.941
0.17	0.149	1.381	1.381

Each edge of the plate is assumed to be simply supported (S); fully clamped (C); or free (F). Four CNT distribution patterns along the thickness

of each layer such as UD, FG-O, FG-V and FG-X are considered. For convenience, the non-dimensional natural frequency is defined as [4]:

$$\bar{\omega}_{mn} = \omega_{mn} \frac{b^2 \sqrt{\rho^m / E^m}}{h} \tag{18}$$

where $\bar{\omega}_{mn}$ is the natural frequency of the laminated FG-CNTRC plate.

Convergence study

To obtain a reasonable accuracy, the first three non-dimensional frequencies are calculated with increasing the polynomial terms (*m*, *n*). Table 3 presents the convergence of the non-dimensional frequency of square anti-symmetric cross-ply $[0^0/90^0]_5$ laminated UD-CNTRC plates under various types of BCs.

As can be observed, the increasing number of polynomial terms improves the accuracy of results which converge at $m = n = 7$.

Table 3: Convergence study of the first three non-dimensional frequency for antisymmetric cross-ply $[0^0/90^0]_5$ square laminated UD-CNTRC plates $(a/h = 10)$

Mode		polynomial terms ($m \times n$)						
		1×1	2×2	3×3	4×4	5×5	6×6	7×7
SSSS	1	19.874	18.069	16.347	15.381	15.344	15.337	15.335
	2	45.315	39.042	34.974	33.389	31.640	31.545	31.537
	3	45.315	39.042	34.974	33.389	31.640	31.545	31.537
CCCC	1	23.549	22.511	21.714	21.705	21.703	21.703	21.703
	2	40.492	38.057	36.314	34.922	34.885	34.869	34.869
	3	40.492	38.057	36.314	34.922	34.885	34.869	34.869
CSCS	1	20.365	19.917	19.198	18.779	18.772	18.771	18.770
	2	38.694	36.768	34.913	33.244	33.196	33.179	33.176
	3	43.125	40.139	36.005	35.043	33.356	33.331	33.299
CFCF	1	16.458	15.908	15.338	15.331	15.329	15.329	15.329
	2	16.884	16.003	15.458	15.450	15.449	15.447	15.447
	3	20.468	19.522	19.389	19.305	19.304	19.206	19.206
SSFF	1	11.877	11.471	11.441	10.718	10.718	10.716	10.716
	2	14.326	13.958	11.782	11.126	11.067	11.059	11.049
	3	20.014	19.522	19.390	19.304	19.304	19.205	19.205

Validation studies

The first validation study is performed for SSSS and CCCC square single-layer UD-CNTRC plates. Table 4 presents the first six non-dimensional frequencies in comparison with those obtained by Zhu et a. [4] using the finite element method. It can be seen that the good agreement exists between the results of the present approach and the results given by Zhu et al. with maximal discrepancy is only 1.73% for the third frequency of SSSS FG-CNTR plate.

Table 5 and Table 6 show a further comparison for laminated UD-CNTR square plates under various boundary condition with input data: $b/a=1;\ b/h=10;\ V_{CNT}^{*}=0.11$. First six non-dimensional frequencies for laminated UD-CNTR antisymmetric cross-ply $[0^0/90^0]_5$ are presented in Table 5, and for laminated UD-CNTR antisymmetric angle-ply $[45^0/-45^0]_5$ are tabulated in Table 6. The present results are compared with those obtained by using the commercial software ANSYS. The element "SHELL-181" is selected to obtain the natural frequencies. The very good agreement is found with the small discrepancy between the results.

Table 4: The non-dimensional frequency of square single-layer UD-CNTRC plates $\left(V_{CNT}^{*}=0.11; a/h=50\right)$

Mode	SSSS			CCCC		
	Present	Zhu [4]	Error %	Present	Zhu [4]	Error %
1	19.216	19.223	0.03%	40.072	39.730	0.86%
2	23.314	23.408	0.4%	44.082	43.876	0.47%
3	34.078	34.669	1.73%	54.207	54.768	1.03%
4	53.609	54.043	0.81%	75.179	74.448	0.97%
5	70.906	70.811	0.13%	99.619	98.291	1.33%
6	72.996	72.900	0.13%	101.926	100.537	1.36%

Table 5: The non-dimensional frequency of square laminated antisymmetric cross-ply $[0^0/90^0]_5$ UD-CNTRC plates with different boundary conditions ($V^*_{CNT}=0.11; a/h=10$)

	Mode	1	2	3	4	5	6
	Present	15.335	31.537	31.537	41.928	50.026	50.029
SSSS	Ansys	15.220	31.135	31.135	41.358	49.119	49.119
	Error %	0.75%	1.27%	1.27%	1.36%	1.81	1.82
	Present	21.703	34.323	34.323	43.642	50.895	50.923
CCCC	Ansys	21.387	34.323	34.323	43.642	50.895	50.923
	Error %	1.45%	1.56%	1.56%	1.59%	1.64%	1.65%
	Present	18.770	33.176	33.299	43.147	50.659	51.147
CSCS	Ansys	18.541	32.678	32.845	42.509	49.835	50.207
	Error %	1.22%	1.50%	1.36%	1.48%	1.63%	1.84%
	Present	15.329	15.447	19.206	27.726	31.262	31.464
CFCF	Ansys	15.107	15.223	19.131	27.445	30.766	30.967
	Error %	1.45%	1.45%	0.39%	1.01%	1.59%	1.58%
	Present	10.716	11.049	19.205	25.653	29.485	29.709
SSFF	Ansys	10.640	10.963	19.095	25.441	29.094	29.310
	Error %	0.71%	0.79%	0.57%	0.83%	1.33%	1.34%

Table 6: The non-dimensional frequency of square laminated antisymmetric angle-ply $[45^0/-45^0]_5$ UD-CNTRC plates with different boundary conditions ($V^*_{CNT}=0.11; a/h=10$)

	Mode	1	2	3	4	5	6
	Present	16.258	31.347	31.347	43.310	48.645	48.901
SSSS	Ansys	16.058	30.835	30.835	42.474	47.729	47.970
	Error %	1.23%	1.63%	1.63%	1.93%	1.88%	1.90%
	Present	21.013	34.590	34.590	46.219	50.228	50.841
CCCC	Ansys	20.634	33.902	33.902	45.227	49.193	49.784
	Error %	1.80%	1.99%	1.99%	2.15%	2.06%	2.08%
	Present	18.751	32.027	33.848	44.698	48.954	50.273
CSCS	Ansys	18.414	31.451	33.174	43.746	48.012	49.235
	Error %	1.79%	1.80%	1.99%	2.13%	1.92%	2.06%
	Present	12.940	17.284	27.733	28.291	32.332	43.922
CFCF	Ansys	12.723	17.016	27.214	27.847	31.721	43.056
	Error %	1.68%	1.55%	1.87%	1.57%	1.89%	1.97%
	Present	5.526	11.279	21.567	25.303	25.463	39.525
SSFF	Ansys	5.467	11.088	21.280	24.904	25.033	38.744
	Error %	1.07%	1.70%	1.33%	1.57%	1.69%	1.98%

Parametric studies

After verifying the proposed method and Matlab's code, the non-dimensional frequency for laminated FG-CNTRC plates is analyzed in detail. The effects of CNT volume fractions, CNT distribution type, CNT fiber orientation, number of layers, length-to-width ratio, width-to-thickness ratio, and boundary conditions on the non-dimensional fundamental frequencies of FG-CNTRC plates are investigated.

The non-dimensional fundamental frequencies of SSSS anti-symmetric cross-ply $[0^0/90^0]_2$, symmetric cross-ply $[0^0/90^0]_s$, anti-symmetric angle-ply $[45^0/-45^0]_2$, and symmetric angle-ply $[45^0/-45^0]_S$ laminated UD-CNTRC plates with various values of *a/h* ratio and CNT volume fraction are tabulated in Table 7. The geometric parameters of the plate are $a/h = 5; 10; 20; 30; 40$ and 50, and $b/a = 2$.

Table 7: The non-dimensional frequency of SSSS cross-ply and angle-ply laminated UD-CNTRC plates with various values of *a/h* ratio and volume fraction of CNT

	V^*_{CNT}	a/h					
		5	10	20	30	40	50
$[0^0/90^0]_2$	0.11	7.860	11.142	12.971	13.429	13.601	13.684
	0.14	8.255	12.054	14.352	14.953	15.183	15.294
	0.17	9.533	13.794	16.002	16.550	16.756	16.855
$[0^0/90^0]_s$	0.11	6.452	7.910	8.487	8.613	8.658	8.680
	0.14	6.889	8.644	9.373	9.534	9.592	9.620
	0.17	8.005	9.777	10.475	10.625	10.680	10.706
$[45^0/-45^0]_2$	0.11	7.689	10.762	12.807	13.518	13.864	14.065
	0.14	8.100	11.637	14.105	14.984	15.416	15.667
	0.17	8.811	13.325	15.811	16.672	17.091	17.334
$[45^0/-45^0]_s$	0.11	7.198	10.180	12.152	12.784	13.078	13.246
	0.14	7.572	10.971	13.367	14.158	14.527	14.737
	0.17	8.953	12.611	15.005	15.770	16.125	16.329

Figure 3 illustrates the effect of CNT volume fraction and *a/h* ratios on non-dimensional fundamental frequencies. For both cross-ply and angle-ply CNT lamination scheme, it can be observed that enrichment of the polymeric matrix with more carbon nanotube results in higher frequencies of the plate. The non-dimensional fundamental frequency increases with increasing value of width-to-thickness ratios; with increasing *a/h* ratio (thinner plates), the gap between symmetric and anti-symmetric cross-ply lamination becomes bigger. It means the influence of volume fraction of CNT on non-dimensional

fundamental frequencies on thin plates is more considerable than that of thick plates. Furthermore, the non-dimensional natural frequencies of anti-symmetric lamination are higher than those of symmetric lamination for UD configuration of CNT distribution of CNTRC plates.

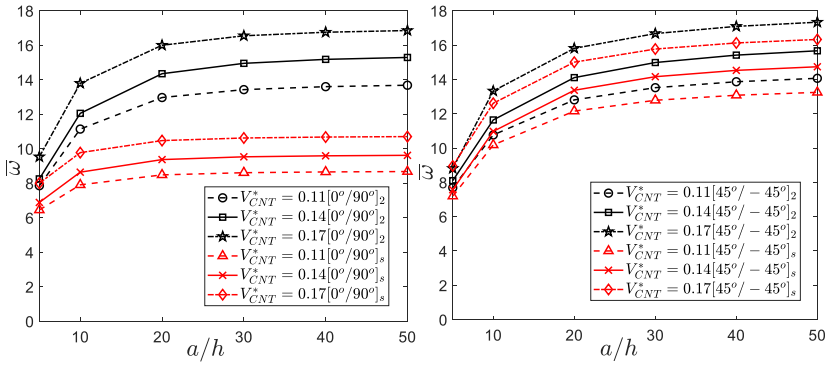

Figure 3: The change of the non-dimensional fundamental frequency of cross-ply and angle-ply laminated UD-CNTRC plates against a/h ratio with different CNT volume fractions

Table 8 presents non-dimensional fundamental frequencies of SSSS anti-symmetric cross-ply $[0^0/90^0]_2$, symmetric cross-ply $[0^0/90^0]_s$, anti-symmetric angle-ply $[45^0/-45^0]_2$, and symmetric angle-ply $[45^0/-45^0]_S$ laminated FG-CNTRC plates with various values of *a/h* ratios, and four different types of SWCNT distribution. The input data are $a/h = 5; 10; 20; 30; 40$ and 50, and $V^*_{CNT} = 0.11$.

Figure 4 depicts the influence of *a/h* ratios and configuration type of SWCNTs on non-dimensional fundamental frequencies. A similar observation can be found from Figure 4: the non-dimensional fundamental frequency increases as *a/h* ratio increases for all types of FG-CNTRC plates. For both cross-ply and angle-ply CNT lamination scheme, it is clearly seen that the FG-O CNTR plates own the lowest non-dimensional frequency and the FG-X CNTR plates own the highest non-dimensional frequency. Thus, to achieve the greater stiffness, the CNTs distributions close to the top and bottom surface of the plate are more efficient than those distributed near the mid-surface. Furthermore, we realize that the fundamental frequencies of the UD type are higher than the FG-V type for both symmetric and antisymmetric laminated FG-CNTR plates.

Table 9 presents the influence of the number of laminae on the non-dimensional fundamental frequency of SSSS anti-symmetric cross-ply and angle-ply UD-CNTRD plates. It is obvious that with a constant thickness, the increase in the number of laminae increases the stiffness of the plate resulting in an increased non-dimensional fundamental frequency of both anti-symmetric cross-ply and angle-ply UD-CNTRD plates.

The effects of angle of CNT orientation on non-dimensional fundamental frequencies of four-edge simply supported antisymmetric angle-ply $[\theta^0/-\theta^0]_2$ and symmetric angle-ply $[\theta^0/-\theta^0]_s$ laminated UD-CNTRC are depicted in Figure 5. The plate with $b/a=2; a/h=10$ and $V^*_{CNT}=0.11$ is investigated. It is seen that the curves are symmetric to the line of $\theta=45^0$ and it corresponds to the maximal values of non-dimensional natural frequencies for both lamination schemes.

Table 8: The non-dimensional fundamental frequency of SSSS cross-ply and angle-ply FG-CNTRC plates with various values of *a/h* ratio and four types of SWCNT distribution (UD, FG-O, FG-V, FG-X) ($V^*_{CNT}=0.11$)

		a / *h*					
		5	10	20	30	40	50
$[0^0/90^0]_2$	UD	7.860	11.142	12.971	13.429	13.601	13.684
	FG-V	7.851	11.091	12.953	13.380	13.573	13.565
	FG-O	7.832	11.039	12.801	13.238	13.402	13.481
	FG-X	7.915	11.264	13.150	13.625	13.804	13.890
$[0^0/90^0]_s$	UD	6.452	7.910	8.487	8.613	8.658	8.680
	FG-V	6.441	7.883	8.453	8.577	8.622	8.643
	FG-O	6.295	7.644	8.173	8.287	8.329	8.348
	FG-X	6.610	8.173	8.799	8.935	8.985	9.008
$[45^0/-45^0]_2$	UD	7.689	10.762	12.807	13.518	13.864	14.065
	FG-V	7.683	10.732	12.752	13.451	13.790	13.986
	FG-O	7.655	10.661	12.642	13.326	13.658	13.851
	FG-X	7.746	10.882	12.984	13.718	14.076	14.284
$[45^0/-45^0]_s$	UD	7.198	10.180	12.152	12.784	13.078	13.246
	FG-V	7.191	10.144	12.076	12.690	12.975	13.137
	FG-O	7.121	10.029	11.920	12.516	12.793	12.945
	FG-X	7.292	10.343	12.387	13.049	13.361	13.541

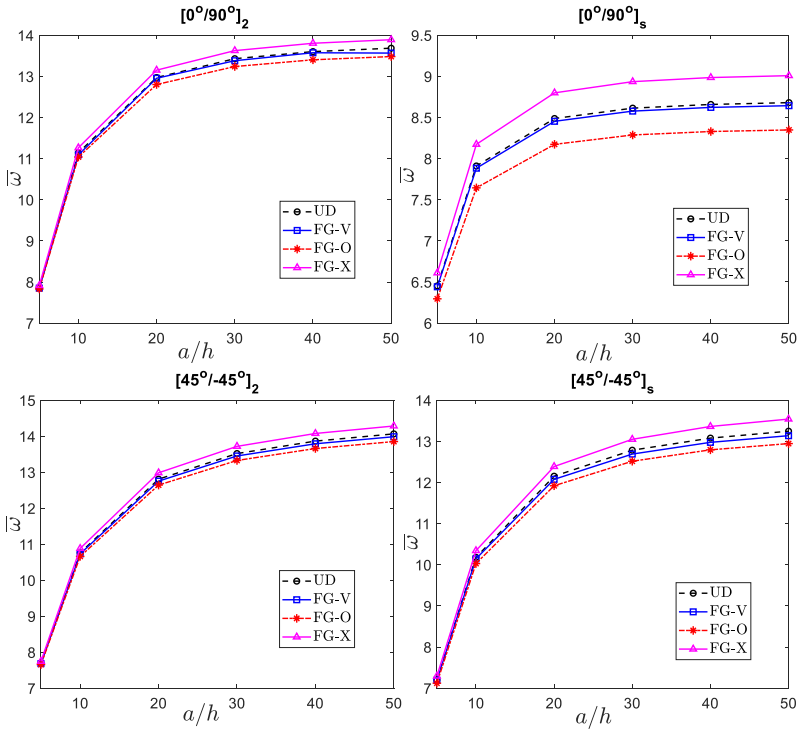

Figure 4: The variation of the non-dimensional fundamental frequency of cross-ply and angle-ply laminated FG-CNTRC plates versus a/h ratio with four types of SWCNT distributions (UD, FG-O, FG-V, FG-X).

Table 9: The non-dimensional fundamental frequency for SSSS antisymmetric cross-ply $[0^0/90^0]_n$ and antisymmetric angle-ply $[45^0/-45^0]_n$ laminated UD -CNTRC plates with different number of lamina

	Number of laminae				
	2	4	6	8	10
$[0^0/90^0]_n$	10.054	11.142	11.224	11.249	11.260
$[45^0/-45^0]_n$	9.232	10.762	10.893	10.934	10.952

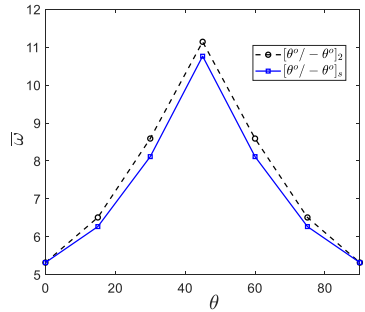

Figure 5: Effects of fiber orientation on the non-dimensional fundamental frequency for SSSS laminated UD-CNTRC plates ($V^*_{CNT} = 0.11$).

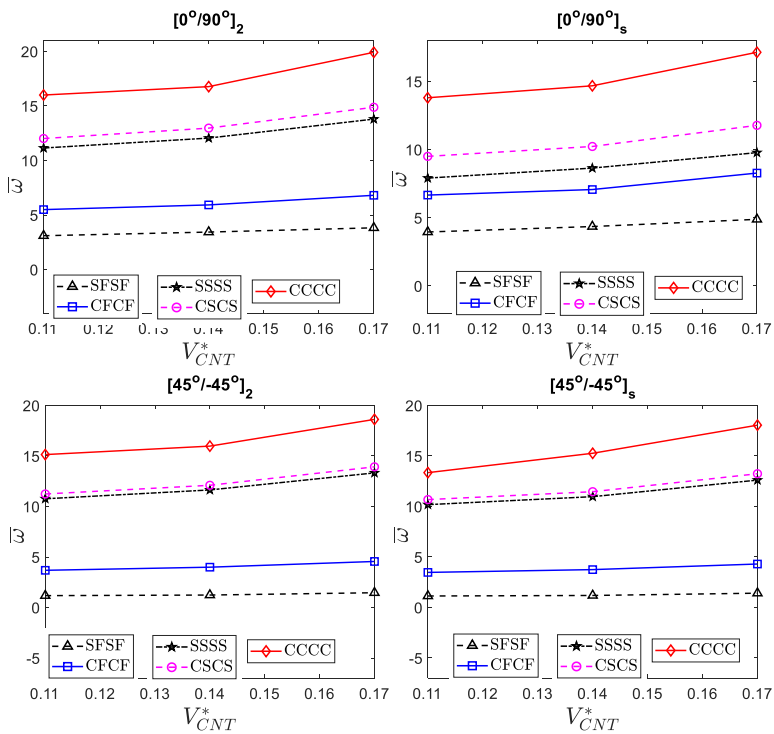

Figure 6: Effects of various BCs on non-dimensional fundamental frequency of laminated UD-CNTRC plates (b/a = 2; a/h = 10; $V^*_{CNT} = 0.11$).

Conclusion

Using the pb2 Rayleigh-Ritz method and based on the FSDT, the free vibration characteristics of FG-CNTRC plates are investigated in this paper. The FG-CNTRC plate is composed of multi-layers that are perfectly bonded. In each layer, four patterns of SWCNTs arrangements including uniform or functionally graded distribution through the thickness are considered. The modified rule of the mixture is used to estimate the effective material properties of the CNTRC. A Matlab's code has been developed and used to validate the present solution against published results. Numerical examples show the significant effects of volume fraction of CNTs, distribution patterns of CNT, thickness to width ratio (*a/h*), aspect ratio (*a/b*), numbers of layers, and boundary conditions on the natural frequencies of FG-CNTRC laminated plates.

Acknowledgement

This research is funded by the National University of Civil Engineering (NUCE) under grant number 23-2020/KHXD-TĐ.

References

[1] S. Iijima, "Helical microtubules of graphitic carbon," *Nature*, vol. 354, pp 56-58, 1991.

[2] M. O. Bidgoli, A. Loghman, and M. Arefi, "Three-Dimensional Thermo-Elastic Analysis of a Rotating Cylindrical Functionally Graded Shell Subjected to Mechanical and Thermal Loads Based on the FSDT Formulation," *Journal of Applied Mechanics and Technical Physics*, vol. 60, pp 899-907, 2019.

[3] M. Omidi Bidgoli, A. Loghman, and M. Arefi, "The Effect of Grading Index on Two-dimensional Stress and Strain Distribution of FG Rotating Cylinder Resting on a Friction Bed Under Thermomechanical Loading," *Journal of Stress Analysis*, vol. 3, pp 75-82, 2019.

[4] P. Zhu, Z. Lei, and K. M. Liew, "Static and free vibration analyses of carbon nanotube-reinforced composite plates using finite element method with first order shear deformation plate theory," *Composite Structures*, vol. 94, pp 1450-1460, 2012.

[5] E. A. Shahrbabaki and A. Alibeigloo, "Three-dimensional free vibration of carbon nanotube-reinforced composite plates with various boundary conditions using Ritz method," *Composite Structures*, vol. 111, pp 362-370, 2014.

[6] M. R. Nami and M. Janghorban, "Free vibration of thick functionally graded carbon nanotube-reinforced rectangular composite plates based on

three-dimensional elasticity theory via differential quadrature method," *Advanced Composite Materials,* vol. 24, pp 439-450, 2015.

[7] R. Ansari, E. Hasrati, M. F. Shojaei, R. Gholami, and A. Shahabodini, "Forced vibration analysis of functionally graded carbon nanotube-reinforced composite plates using a numerical strategy," *Physica E: Low-dimensional Systems and Nanostructures,* vol. 69, pp 294-305, 2015.

[8] B. Selim, L. Zhang, and K. M. Liew, "Vibration analysis of CNT reinforced functionally graded composite plates in a thermal environment based on Reddy's higher-order shear deformation theory," *Composite structures,* vol. 156, pp 276-290, 2016.

[9] L. Zhang, Z. Lei, and K. M. Liew, "Free vibration analysis of functionally graded carbon nanotube-reinforced composite triangular plates using the FSDT and element-free IMLS-Ritz method," *Composite Structures,* vol. 120, pp 189-199, 2015.

[10] L. Zhang, W. Cui, and K. M. Liew, "Vibration analysis of functionally graded carbon nanotube reinforced composite thick plates with elastically restrained edges," *International Journal of Mechanical Sciences,* vol. 103, pp 9-21, 2015.

[11] L. Zhang, Z. Lei, and K. M. Liew, "Vibration characteristic of moderately thick functionally graded carbon nanotube reinforced composite skew plates," *Composite Structures,* vol. 122, pp 172-183, 2015.

[12] L. Zhang and B. Selim, "Vibration analysis of CNT-reinforced thick laminated composite plates based on Reddy's higher-order shear deformation theory," *Composite Structures,* vol. 160, pp 689-705, 2017.

[13] A. Alibeigloo and A. Emtehani, "Static and free vibration analyses of carbon nanotube-reinforced composite plate using differential quadrature method," *Meccanica,* vol. 50, pp 61-76, 2015.

[14] L. Zhang, Z. Song, and K. M. Liew, "State-space Levy method for vibration analysis of FG-CNT composite plates subjected to in-plane loads based on higher-order shear deformation theory," *Composite Structures,* vol. 134, pp 989-1003, 2015.

[15] R. Ansari, J. Torabi, and R. Hassani, "A comprehensive study on the free vibration of arbitrary shaped thick functionally graded CNT-reinforced composite plates," *Engineering Structures,* vol. 181, pp 653-669, 2019.

[16] Y. Kiani, "Free vibration of FG-CNT reinforced composite skew plates," *Aerospace Science and Technology,* vol. 58, pp 178-188, 2016.

[17] M. Wang, Z. M. Li, and P. Qiao, "Semi-analytical solutions to buckling and free vibration analysis of carbon nanotube-reinforced composite thin plates," *Composite Structures,* vol. 144, pp 33-43, 2016.

[18] N. D. Duc, J. Lee, T. Nguyen Thoi, and P. T. Thang, "Static response and free vibration of functionally graded carbon nanotube-reinforced composite rectangular plates resting on Winkler–Pasternak elastic

foundations," *Aerospace Science and Technology,* vol. 68, pp 391-402, 2017.

[19] T. Truong Thi, T. Vo Duy, V. Ho Huu, and T. Nguyen Thoi, "Static and free vibration analyses of functionally graded carbon nanotube reinforced composite plates using CS-DSG3," *International Journal of Computational Methods,* vol. 17, pp 1850133, 2020.

[20] Z. Lei, L. Zhang, and K. M. Liew, "Free vibration analysis of laminated FG-CNT reinforced composite rectangular plates using the kp-Ritz method," *Composite Structures,* vol. 127, pp 245-259, 2015.

[21] P. Malekzadeh and A. Zarei, "Free vibration of quadrilateral laminated plates with carbon nanotube reinforced composite layers," *Thin-Walled Structures,* vol. 82, pp 221-232, 2014.

[22] C. P. Wu and H. Y. Li, "Three-dimensional free vibration analysis of functionally graded carbon nanotube-reinforced composite plates with various boundary conditions," *Journal of Vibration and Control,* vol. 22, pp 89-107, 2016.

[23] P. Malekzadeh and Y. Heydarpour, "Mixed Navier-layerwise differential quadrature three-dimensional static and free vibration analysis of functionally graded carbon nanotube reinforced composite laminated plates," *Meccanica,* vol. 50, pp 143-167, 2015.

[24] B. Huang, Y. Guo, J. Wang, J. Du, Z. Qian, T. Ma, *et al.*, "Bending and free vibration analyses of antisymmetrically laminated carbon nanotube-reinforced functionally graded plates," *Journal of Composite Materials,* vol. 51, pp 3111-3125, 2017.

[25] Z. Lei, L. Zhang, and K. M. Liew, "Analysis of laminated CNT reinforced functionally graded plates using the element-free kp-Ritz method," *Composites Part B: Engineering,* vol. 84, pp 211-221, 2016.

[26] H. S. Shen, "Nonlinear bending of functionally graded carbon nanotube-reinforced composite plates in thermal environments," *Composite Structures,* vol. 91, pp 9-19, 2009.

[27] J. Wang and R. Pyrz, "Prediction of the overall moduli of layered silicate-reinforced nanocomposites—part I: basic theory and formulas," *Composites Science and Technology,* vol. 64, pp 925-934, 2004.

[28] J. Fidelus, E. Wiesel, F. Gojny, K. Schulte, and H. Wagner, "Thermo-mechanical properties of randomly oriented carbon/epoxy nanocomposites," *Composites Part A: Applied Science and Manufacturing,* vol. 36, pp 1555-1561, 2005.

[29] J. N. Reddy, *Mechanics of laminated composite plates and shells: theory and analysis*: CRC press, 2004.

[30] H. S. Shen, "Nonlinear bending of functionally graded carbon nanotube-reinforced composite plates in thermal environments," *Composite Structures,* vol. 91, pp 9-19, 2009.